Metrol. Meas. Syst., Vol. 33 (2026) No. 1, pp. 1–17
DOI: 10.24425/mms.2026.158373

PAN POLSKA AKADEMIA NAUK

METROLOGY AND MEASUREMENT SYSTEMS
Index 330930, ISSN 0860-8229
www.metrology.wat.edu.pl

M&MS

IMPROVING THE TAGG'S SLOPE METHOD FOR LARGE-SCALE GROUNDING SYSTEMS THROUGH FINITE ELEMENT METHOD SIMULATIONS

Miguel Martínez-Lozano

Technical University of Madrid, School of Industrial Engineering, Department of Automation, Electrical and Electronic Engineering and Industrial Computing, Spain (✉ *miguel.mlozano@upm.es*)

Abstract

Measurement of the grounding resistance of very large installations is difficult because conventional fall-of-potential methods require impractically long test leads. The Tagg slope method reduces this distance, but its traditional formulation neglects finite electrode dimensions and relies on curve extrapolations outside the range originally analysed, leading to large errors.This paper revises the method using finite element simulations that model realistic electrode geometry and soil conduction. A new relationship between the slope of the voltage profile and the position of the measuring electrode is obtained and fitted by a polynomial with errors below 0.02%. The corrected method is tested on large square grounding grids and on a photovoltaic-plant grounding system. Results show that, when measurements are taken away from corner regions and with auxiliary-electrode distances above about 20% of the system diagonal, the grounding resistance can be estimated with errors below 3%, while the traditional implementation may produce errors of up to 60.

Keywords: rounding resistance measurement, Large grounding systems, renewable plants, Fall-of-Potential Method (FOPM), Tagg Slope Method (TSM), Finite Element Method (FEM).

1. Introduction

Grounding systems are essential for electrical safety and continue to be an active research area, particularly with regard to soil resistivity, electrode design, and resistance verification [1–4]. However, conventional *Fall-of-Potential* (FOP) methods require large auxiliary-electrode spacings that are often impractical. In urban environments [4] and in large renewable facilities such as photovoltaic and wind plants [5], limited space and long test-leads introduce inductive effects and large measurement errors. Although there are several alternative impedance-measurement techniques [6], most lack broad industrial acceptance without strong validation. As a result, accurately measuring grounding resistance in these scenarios remains challenging and motivates the review of current methodologies [3].

This study focuses on the methodology proposed by Tagg [7, 8], adopted in IEEE Std 81 [1, 3] to measure large grounding systems and commonly referred to as the *Tagg Slope Method* (TSM).

Article history: received August 20, 2025; revised January 13, 2026; accepted February 10, 2026; available online March 13, 2026.

This method enables grounding resistance measurements using the *Fall-of-Potential Method* (FoPM) but with *current electrode* (CE) distances shorter than those required by the conventional approach. The technique relies on obtaining a voltage profile using a distant CE and a *potential electrode* (PE), determining the slope μ of this profile, and applying a correction to identify the theoretical PE position that produces the correct resistance measurement.

IEEE Std 81 [1] includes this approach in a dedicated section and provides a correction table (Table 5) for μ values between 0.4 and 1.6, originally derived from Tagg's work [7, 8]. The draft of the upcoming IEEE revision [3] replaces this table with a fourth-order polynomial curve fit, extending only the upper limit ($\mu < 2$). However, this curve fitting does not accurately represent the theoretical behaviour in the range $1.6 < \mu < 2$, as it extrapolates from data within $0.4 < \mu < 1.6$ without incorporating Tagg's original equation in the extended range.

Recent studies have highlighted inconsistencies in TSM, especially when μ exceeds the IEEE tabulated range or when analytical assumptions depart from realistic electrode geometry [9–14]. These issues motivate a re-evaluation of the method.

Furthermore, [14] introduces correction factors to account for deviations from the original methodology, demonstrating that the Tagg Slope Method still requires a deeper examination. These findings highlight the need for a more robust theoretical foundation to better define its practical limitations.

However, key issues remain. Tagg's original formulation imposes the constraint $0.5714 < \mu < 2$, which is not respected in the current IEEE range, and the simplification of modelling the CE as a point neglects the influence of its radius on the potential distribution.

In this work, these limitations are addressed through *finite element method* (FEM) simulations of hemispherical configurations, solving the Poisson's equation under electrostatic conditions to account for soil conductivity. The simulations enable a re-evaluation and correction of Tagg's results, leading to an updated equation to determine the effective PE position as a function of μ. The study further applies this analysis to some practical grounding configurations: a long square mesh and a *photovoltaic* (PV) plant. This work reviews TSM using finite element simulations and evaluates its performance in large grounding systems.

2. Theoretical background

2.1. Measurement of Grounding Resistance Using the Tagg Slope Method

The TSM is a specific implementation of the FoPM [1, 7]. As shown in Fig. 1, a current I is injected into the electrode under test (E), and returned through the auxiliary current electrode CE, located at distance C. The PE is then moved along the y-axis to obtain R_m, defined as the voltage difference between E and PE divided by I. From the resulting potential distribution, the grounding resistance R_E of the electrode can be estimated.

From an analytical point of view [7, 8], Tagg modelled the electrode E as a hemisphere of radius r, with the auxiliary CE placed at a distance C and the PE at a distance P. When a current I is injected between E and CE, a potential is developed at the electrode E given by (1), and an analogous potential appears at the electrode PE, as expressed in [7]:

$$\upsilon E = \frac{\rho \cdot I}{2\pi} \cdot \left[\frac{1}{r} - \frac{1}{C}\right], \tag{1}$$

$$\upsilon PE = \frac{\rho \cdot I}{2\pi} \cdot \left[\frac{1}{P} - \frac{1}{C-P}\right]. \tag{2}$$

Metrol. Meas. Syst., Vol. 33 (2026), No. 1, pp. 1–17
DOI: 10.24425/mms.2026.158373

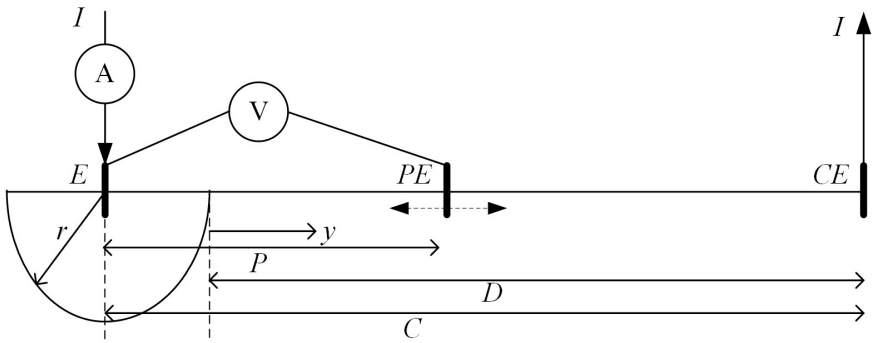

Fig. 1. Spatial scheme.

The potential difference between these two points, denoted V_m, is given by (3). Dividing this value by the current I result in the measured resistance R_m, expressed in (4), which is a function of the position P of the auxiliary potential electrode PE:

$$V_m = \upsilon E - \upsilon PE = \frac{\rho \cdot I}{2\pi} \cdot \left[\frac{1}{r} - \frac{1}{C} - \frac{1}{P} - \frac{1}{C-P}\right], \tag{3}$$

$$R_m = \frac{V_m}{I} = \frac{\rho}{2\pi} \cdot \left[\frac{1}{r} - \frac{1}{C} - \frac{1}{P} - \frac{1}{C-P}\right]. \tag{4}$$

As shown in Fig. 2, the potential-drop profile depends on the spacing C between the test electrode E and the auxiliary current electrode CE. Since both electrodes contribute to the measured potential, the FoPM requires C to be sufficiently large for their fields not to overlap [7]. When $C \gg r$, typically 5–10 r, the potential profiles resemble the case $C1$ in Fig. 2, and R_E can be

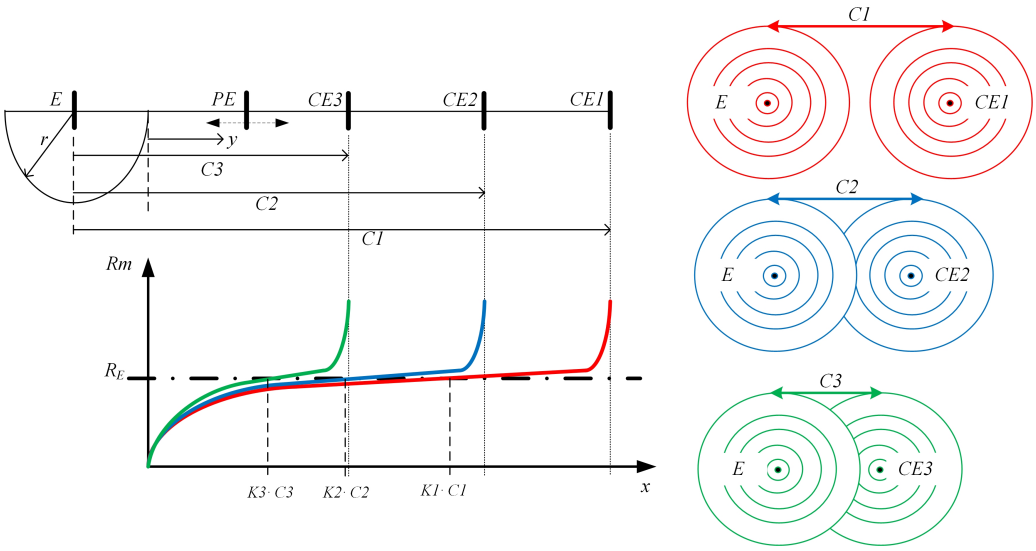

Fig. 2. Fall-of-potential method.

obtained from the R_m curve by placing the potential electrode at approximately 61.8% of C (K_1 = 0.618). In contrast, for smaller separations such as $C2$ (and similarly $C3$) the potential profiles overlap significantly, preventing the direct application of the FoPM and making it necessary to use alternative techniques such as the TSM.

The slope method establishes the following procedure: for a distance $C3$, three measurements of R_m are taken at different positions P of the electrode PE: the first at 0.2 times $C3$ (R_{m1}), the second at 0.4 (R_{m2}) and the third at 0.6 (R_{m3}). The relationship among these three points is [7] and [8] the slope μ and is determined by

$$\mu = \frac{R_{m3} - R_{m2}}{R_{m2} - R_{m1}}. \tag{5}$$

Tagg derived a closed-form solution to (4) by using three points of the FoPM curve to obtain a quadratic expression that identifies the position at which the calculated resistance matches the theoretical value. He initially proposed using measurements at 0.4, 0.6, and 0.8 C [7], later extending the range to 0.2–0.8 C [8]. The approach adopted in IEEE standards [1–3], and followed in this work, uses the three measurements at 0.2, 0.4, and 0.6 C to solve (4).

Once μ is known, the corresponding PE position can be obtained from Tagg's solution to (4) [7, 8]. In (4), the first term gives the true grounding resistance R_E, while the remaining terms represent the measurement error. Using the three measured values R_{m1}, R_{m2}, and R_{m3}, Tagg determined the PE location at which this error becomes zero. Because the result depends solely on μ for uniform soils, the IEEE standard [1] provides the corresponding PE positions in Table 5 of [1], summarised in Table 1.

Table 1. Some representative data from Table 5 [1] establishing the position of PE for a value of m.

μ	***PE* position***	μ	***PE* position***
0.40	0.643	0.5	0.629
0.75	0.589	1	0.542
1.5	0.389	1.59	0.341

*The PE position is expressed as per unit of the current electrode position or distance (CE).

The updated IEEE 81 draft [3] introduces a curve-fitted expression derived directly from the tabulated values, given in (6). A similar curve-fitting approach is also presented in [10] and [11], whose corresponding expressions are:

$$P/C = -0.1357 \cdot \mu^4 + 0.4196 \cdot \mu^3 - 0.5395 \cdot \mu^2 + 0.1509 \cdot \mu + 0.646, \tag{6}$$

$$P/C = -0.1242 \cdot \mu^3 + 0.2339 \cdot \mu^2 - 0.3049 \cdot \mu + 0.738, \tag{7}$$

where P/C is the ratio between the position at which the electrode PE must be placed and the distance to the CE electrode C. Neither [3] nor [10] report the correlation parameters or the fitting errors associated with their curve-fitting procedures.

2.2. Considerations and Limitations

The TSM relies on simplified assumptions, including neglecting electrode dimensions, which introduces systematic errors at short electrode spacings. This motivates the need for a corrected formulation. Tagg's potential expression omits the radius of the hemispherical electrode [7], which is corrected:

Metrol. Meas. Syst., Vol. 33 (2026), No. 1, pp. 1–17
DOI: 10.24425/mms.2026.158373

$$\upsilon E = \frac{\rho \cdot I}{2\pi} \cdot \left[\frac{1}{r} - \frac{1}{C-r}\right]. \tag{8}$$

The analytical model also neglects the radius of the auxiliary electrode r_{CE}, further reducing the accuracy for small spacings. FEM simulations are therefore required to obtain corrected slope-method factors beyond those in Table 1 and expressions (6) and (7).

From (4), as illustrated in Fig. 3a, the theoretical bounds are $0.5714 < \mu < 2$, yet IEEE 81 provides values only for $0.4 < \mu < 1.6$, creating inconsistencies with the analytical basis of the method.

The curve-fitting formulas in [3, 10, 11], based solely on the IEEE Table 5 dataset [1] (Table 1), do not reproduce the analytical solution for $\mu > 1.6$, with deviations up to 60%.

As illustrated in Fig. 3b, the 'IEEE' data [1] are strictly confined to the range $0.4 < \mu < 1.6$, while 'P81/D4' [3] (6) and 'PUB' [10, 11] (7) performed a curve fitting based on data, extrapolating erroneously to the range to $0.6 < \mu < 1.9$. The 'Analyt' set represents the exact solution of (4). Notice that the anomalous point in the IEEE curve [1] at $\mu = 0.92$ is the result of a typographical error in the standard.

Using the analytical solution of (4), a complete μ vs *P/C* dataset was generated and fitted with the fifth-order polynomial (9), achieving a correlation of 0.9996:

$$P/C = -0.9026 \cdot \mu^5 + 4.824 \cdot \mu^4 - 10.17 \cdot \mu^3 + 10.41 \cdot \mu^2 - 5.314 \cdot \mu + 1.696. \tag{9}$$

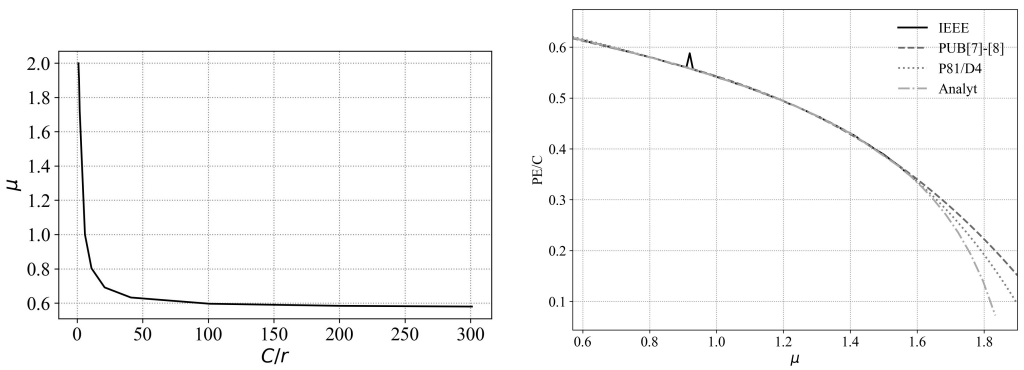

Fig. 3. Considerations about μ: a) analytical limits of μ and b) Differences in the curve fitting process.

The limitations of the TSM as defined in the current standards justify the revised approach proposed here. The following methodology updates the *P/C* values using FEM simulations with hemispherical electrodes, preserving Tagg's original concept. The corrected *P/C* data are then applied to three case studies to validate their performance for large, complex grounding systems typical of utility-scale renewable plants.

3. Proposed methodology

This section derives the *P/C*–μ relationship, determining the required position of PE as a function of μ following Tagg's original principles [7, 8], but using finite element simulations rather than simplified analytical formulas. The analysis employs *ANSYS Electronic Desktop*

2025 R2. Two hemispherical electrodes, E (radius r) and CE (radius r_{CE}), separated by distance C are modelled, and a 1 A current is injected between them to obtain the potential profile along the line that joins their centres. The geometry and dimensions used are shown in Fig. 4.

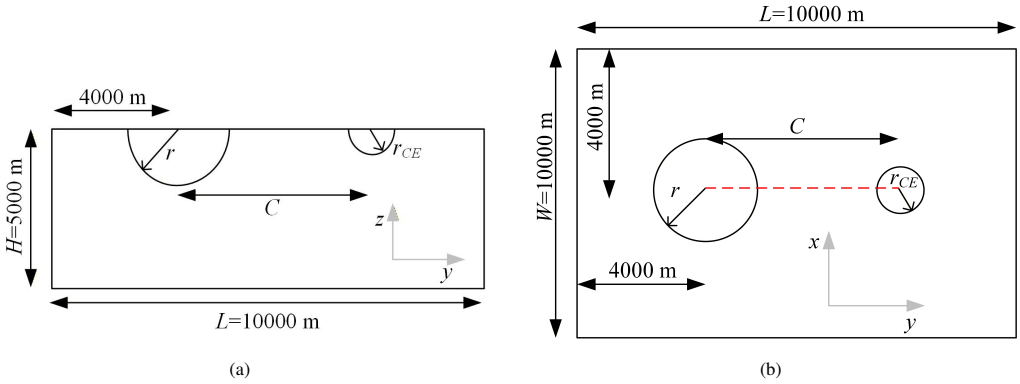

Fig. 4. Geometry used for the methodology: a) cross section and b) plan view.

The problem was solved using the finite element method [15, 16] with an electroquasistatic formulation to solve the small electric currents in conductive media (σ, $\rho = 1/\sigma$). The governing equation is the charge conservation law expressed by

$$\nabla \cdot (\sigma \nabla V + j\omega\varepsilon \nabla V + Je) = 0, \tag{10}$$

where V is the electric potential, σ the electrical conductivity, ε the permittivity, and Je an externally applied current density. The electric field is given by

$$E = -\nabla V, \tag{11}$$

and the total current density by

$$J = \sigma E + j\omega\varepsilon E. \tag{12}$$

The model uses a prescribed current source and zero-potential (Dirichlet) conditions on the outer boundaries. The computational domain was sized (L = 10000 m, W = 10000 m, H = 5000 m) to avoid the boundary influence on the potential. The applied boundary conditions are shown in Fig. 5.

3.1. Scenarios considered

To obtain a general *P/C* vs μ correlation, multiple simulation scenarios were defined considering the key parameters that affect the potential profile, as summarised in Table 2.

All simulations used the same parameters: a 1 A injected current, uniform soil resistivity of 100 Ω·m, the defined domain dimensions, and grounded external boundaries. A refined mesh (~350,000 nodes and 3 million DOF) was constructed to accommodate the geometric scale differences, following accepted FEM practices for electrical problems [17–19]. Additionally, a preliminary simulation without the CE electrode was performed to obtain the reference resistance $R_{E,FEM}$ for each value of r.

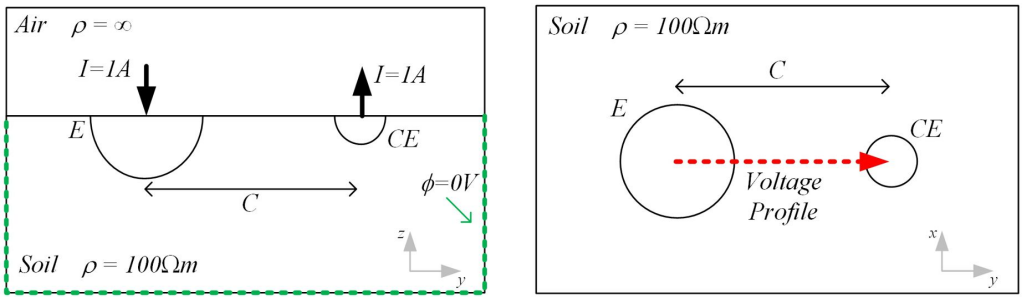

(a) (b)

Fig. 5. Boundary conditions defined in the problem statement: a) cross section and b) plan view.

Table 2. Scenarios considered for the simulations.

Variable	Range
r (radius of the electrode E) [m]	100, 200, 300 and 500
rCE (radius of the electrode CE) [m]	0.1, 0.5, 1
C (distance between E and CE) [m]	1.1, 1.2, 1.3, 1.4, 1.5, 1.6, 1.7, 1.8, 1.9, 2, 2.25, 2.5, 2.75, 3, 3.25, 3.5, 3.75, 4, 4.5, 5, 6, 7, 8, 9, 10, 10, 20 times r

3.2. Analysis of the scenarios considered

For each scenario, the potential profile along the y-axis was computed between the effective boundaries of the electrodes E and CE, *i.e.*, from $d = 0$ at the edge of E to $d = C - (r + r_{CE})$ at the edge of CE, excluding the constant-potential regions. The potentials are positive near E (where the current enters) and negative near CE (where it exits). To express the data in the form required for the FPM, the profile is shifted by adding υ_E and inverted so that $V_m = 0$ at $d = 0$, producing the corresponding R_m profile used in the analysis. The resulting transformation is illustrated in Fig. 6.

For each scenario, the intersection between the measured R_m profile and the FEM-based reference $R_{E,FEM}$ gives the normalised position P/d, while the slope μ is computed from (5). These values are combined to obtain a general P/d function suitable for field use, replacing the original Tagg-based procedure in IEEE 81 [1,3]. Because d coincides with the measurable zero-reference of R_m, it provides a more practical distance variable than C, as further discussed in the results section.

4. Results

4.1. Voltage profiles

Figure 8 shows the FEM-computed voltage profiles for the hemispherical electrodes E and CE for several separation distances d. These profiles illustrate the influence of electrode proximity on potential-field superposition, a key factor that affects FoPM-based techniques, and the 61.8% rule. Although Fig. 7b and Fig. 7c presents the case of $r = 100$ m and $r_{CE} = 1$ m, the same qualitative behaviour is observed for all values of r, both in the potential distribution and the resulting R_m curves.

As shown in Fig. 7a, the voltage profiles are extracted along the y-axis at $x = 0$ and $z = 0$, from the edge of the electrode E up to 1500 m, covering the full range of relevant separations d.

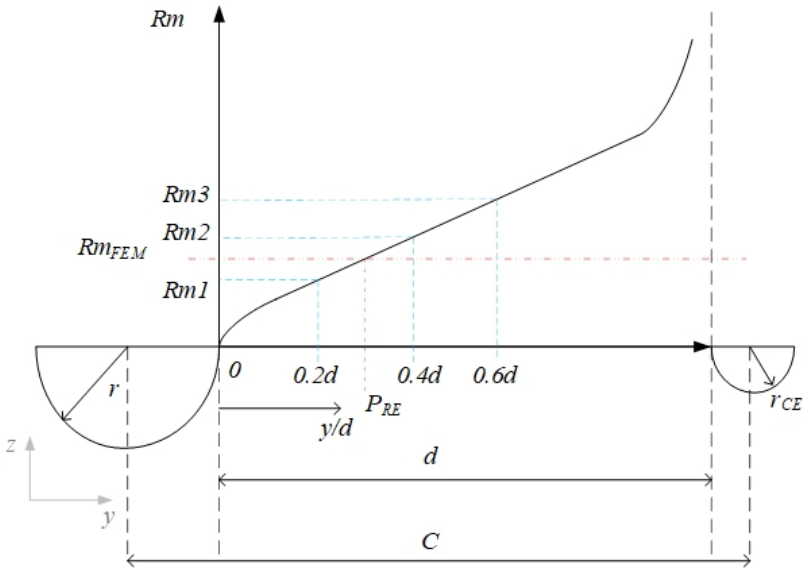

Fig. 6. Results of typical simulations for data extraction and analysis.

Decreasing d increases the superposition area, while larger values of d approach the ideal FoPM behaviour illustrated in Fig. 2. For each scenario, the correct potential-electrode PE location is obtained by intersecting the simulated profile with the theoretical resistance RE_t; this intersection, normalised as y/d, provides the corresponding theoretical PE position.

4.2. Measured resistance (Rm) profile behaviour as a function of distance (d)

Once the potential profiles are obtained for each combination of r, r_{CE}, and separation d, they are converted to the corresponding R_m profiles. Using the theoretical resistance RE_t for hemispherical electrodes in uniform soil (13), the intersection between R_m and RE_t yields the normalised position P/d at which the PE should be placed. Figures 8 and 9 summarise the behaviour of P/d across the specific scenarios with r =100 m and r = 500 m.

$$RE_t = \frac{\rho}{2 \cdot \pi} \cdot \left(\frac{1}{r}\right). \tag{13}$$

The theoretical value of RE_t for the different scenarios studied is presented in Table 3.

Table 3. Evaluation of *REt* for various values of *r*.

***r* [m]**	100	200	300	500
***REt* [Ω]**	0.16	0.08	0.05	0.03

For large d, the intersection converges to the classical 61.8% position defined in the IEEE FoPM [1,3], while for smaller d the optimal PE location progressively shifts toward the electrode E.

Metrol. Meas. Syst., Vol. 33 (2026), No. 1, pp. 1–17
DOI: 10.24425/mms.2026.158373

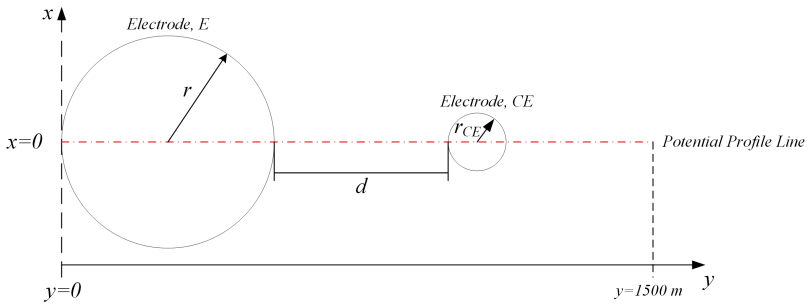

(a)

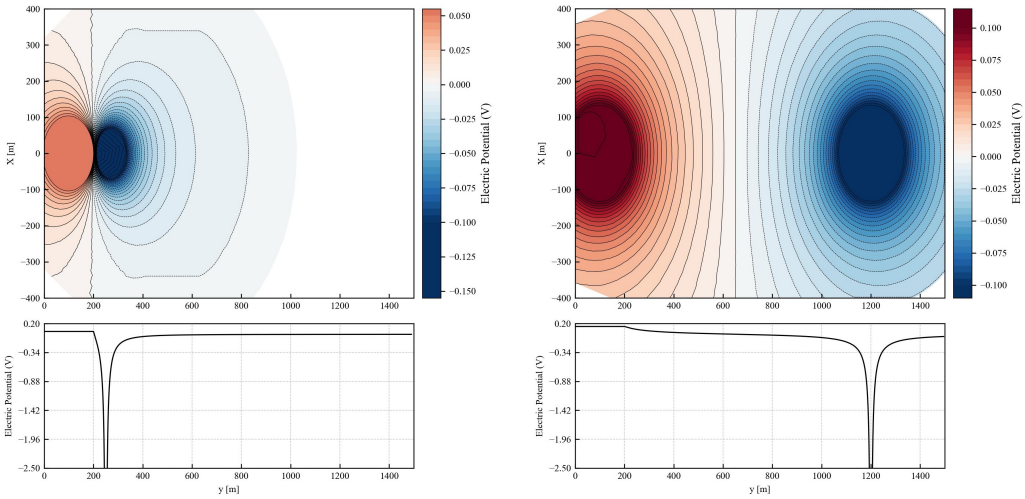

(b) (c)

Fig. 7. Voltage profile a) Geometrical description, b) d=50 m, c) d=1500 m.

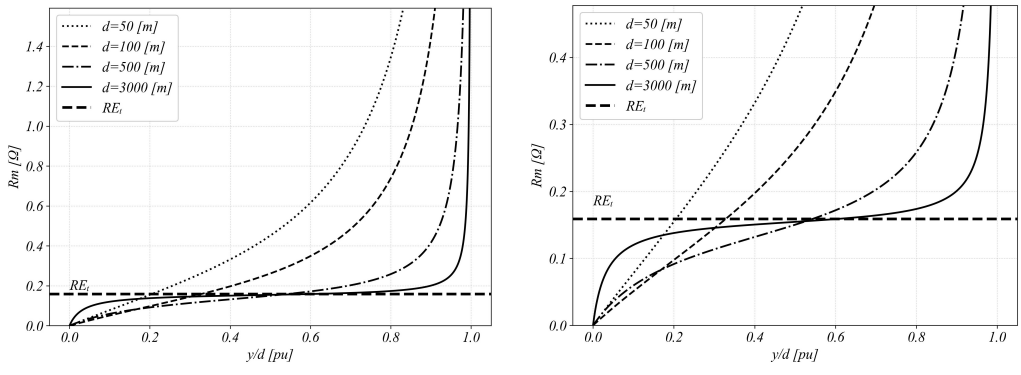

(a) (b)

Fig. 8. R_m for r = 100 m for various distances d: a) full potential profile, b) detail near the theoretical resistance intersection.

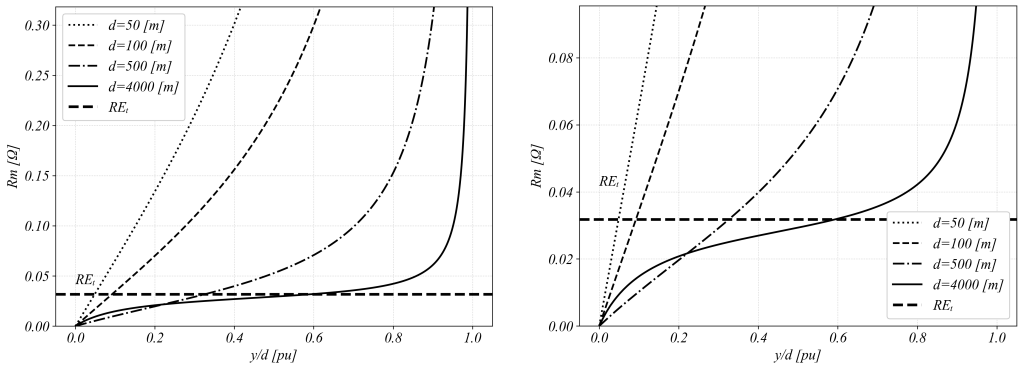

Fig. 9. R_m for r = 500 m for various distances d: a) full potential profile, b) detail near the theoretical resistance intersection.

4.3. Analysis of data for a functional relationship between the Potential Electrode Position (P/d) and the slope (μ)

In all simulation scenarios, a consistent relationship is observed between the slope μ, computed following Tagg [8] and IEEE procedures [1–3] using (5), and the normalised PE location *P/d*. For each FEM model, *P/d* is obtained from the intersection between the simulated R_m profile and the theoretical resistance, and the aggregated results are shown in Fig. 10 (*P/d* – FEM). Figure 11 also compares these FEM data with the fitting expressions (6) and (9), revealing significant deviations reported in the literature for $\mu > 1.4$, which arise when d becomes very small. These discrepancies motivate the derivation of a new curve-fitted expression that improves the estimation of *P/d* and addresses the limitations noted in [10, 11, 13] and in the IEEE draft [3].

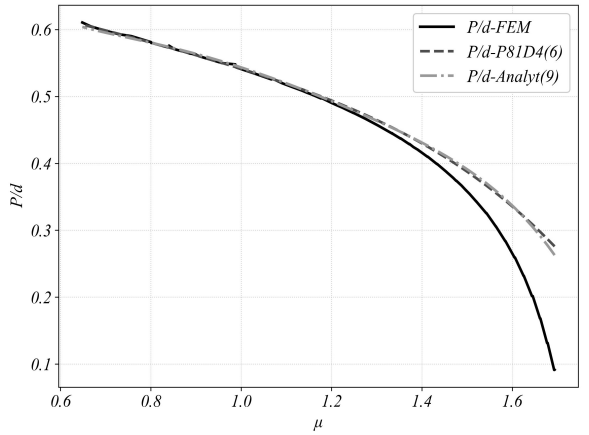

Fig. 10. P/d vs μ.

Based on the μ vs *P/d* dataset shown in Fig. 10, a fifth-order polynomial fit consistent with the IEEE formulation style was obtained, achieving a correlation of 0.9998. The resulting expression is given as

$$P/d = -3.4448 \cdot \mu^5 + 18.73 \cdot \mu^4 - 40.233 \cdot \mu^3 + 42.432 \cdot \mu^2 - 22.088 \cdot \mu + 5.149. \qquad (14)$$

Metrol. Meas. Syst., Vol. 33 (2026), No. 1, pp. 1–17
DOI: 10.24425/mms.2026.158373

5. Application to Case Studies

5.1. Description of cases

A key goal of this work is to show that the corrected methodology can be reliably applied to large-scale grounding systems, including those found in renewable energy facilities. To demonstrate this, the following section applies the method to three representative case studies using FEM simulations, providing a detailed evaluation of its accuracy and its advantages over conventional measurement approaches:

– Case 1: A square grounding grid with a 500 m side,
– Case 2: A square grounding grid with a 1000 m side, and
– Case 3: A typical simplified grounding arrangement of a utility-scale photovoltaic plant.

In all three scenarios, the electrode E is modelled as a 5-cm-radius copper conductor buried 2 m deep (Fig. 11a), and the current electrode CE as a 1-m-radius hemispherical electrode. All simulations assume a uniform soil resistivity of 100 Ω·m, a 1 A injected current, and remote boundaries at zero potential. For square grids (L = 500 m and 1000 m), two measurement profiles are considered - one originating from a corner and another from the midpoint of a side (Fig. 11b). The photovoltaic-plant model (Fig. 11c) consists of five 1000-m branches connected to a 50×100 m substation mesh, with the profile taken from a substation corner. In every case, the voltage is obtained along a straight line from the selected point on E toward CE, converted into R_m, and compared with the theoretical resistance of each geometry, obtained from an additional FEM simulation using only the *ground-potential rise* (GPR). The resulting intersection provides the corresponding P/d, which is then evaluated against the corrected slope-method prediction given by (14).

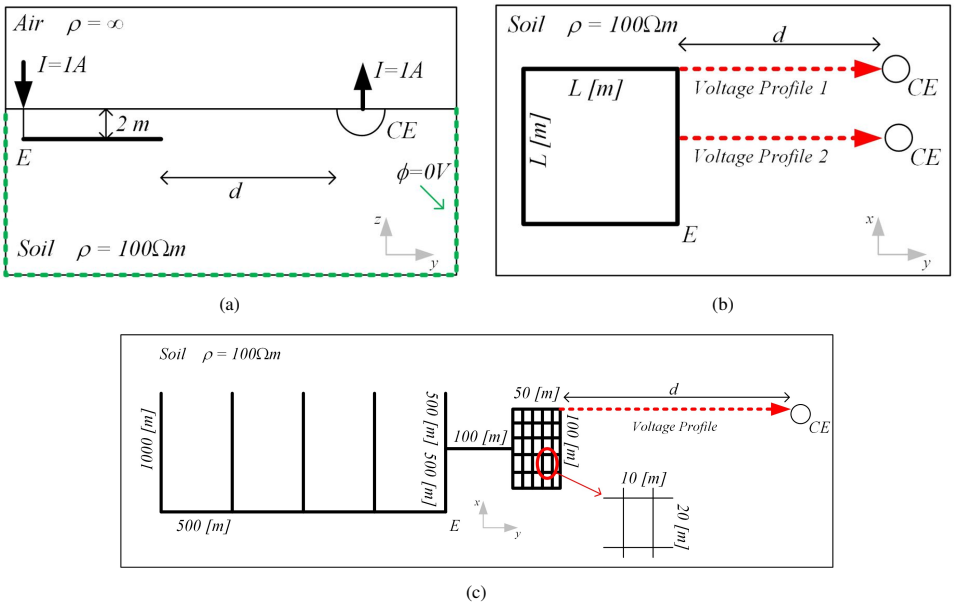

Fig. 11. Geometry used for the studied cases: a) general characteristics of burial depth and soil conditions, b) schematic layout and voltage profiles for the square grid, and c) overall layout and voltage profiles for the photovoltaic plant.

5.2. Case 1: Results

For *Case 1*, corresponding to the 500 m × 500 m grid shown in Fig. 11, the FEM-computed potential profiles were obtained for $d = \{100, 250, 500, 1000, 1500, 3000\}$ m, as illustrated in Fig. 12 for both measurement profiles. The difference between *Profile 1* (corner-based) and *Profile 2* (mid-side) is noticeable only for very small separations, mainly for $\mu < 100$ m, which corresponds to *d/DIAG* < 0.14 for this grid; therefore, this range is excluded from the subsequent analysis (*DIAG* is the diagonal distance of the square mesh as illustrated in Fig. 13).

The reference resistance for this case, $RE_t = 0.117\ \Omega$, was obtained from FEM. For each separation d, the intersection between R_m and RE_t provided P/d_t, while the slope μ was computed from (5) and used to estimate the expected PE position using both the IEEE formulation [3] and the expression based on FEM. The predicted positions were mapped onto the corresponding R_m curves to determine the estimated resistances, and the errors were evaluated using:

$$Error\ (\%) = \left| \frac{RE_m - RE_t}{RE_t} \right| \cdot 100. \tag{15}$$

Tables 4 and 5 show that the IEEE method exhibits large errors when $\mu > 1.4$, whereas both formulations perform similarly for $0.6 < \mu < 1.4$, consistent with the μ-d trend in Fig. 12. They also highlight the effect of the measurement path: corner-based measurements (*Profile 1*) are more sensitive to distortion at small d, yielding average errors near 5%, while mid-side measurements (*Profile 2*) keep errors below 2.5%. Finally, the corrected TSM provides reliable estimates even for $d/DIAG \approx 0.2$, as shown in Fig. 13, enabling practical reduced-distance measurements with the CE placed near the grid boundary.

Table 4. Results for Case 1 (*Voltage Profile* 1).

d [m]	*d/DIAG*	μ	*P/dt*	*P/d* (IEEE)	RE_m (IEEE)	*P/d* (FEM)	RE_m (FEM)	Error [%] (IEEE)	Error [%] (FEM)
100	0.141	1.667	0.143	0.294	0.185	0.118	0.105	57.89	10.16
250	0.354	1.523	0.327	0.377	0.128	0.321	0.116	9.55	0.50
500	0.707	1.335	0.477	0.453	0.114	0.431	0.111	2.48	5.11
1000	1.414	1.099	0.587	0.519	0.111	0.515	0.110	5.51	5.88
1500	2.121	0.963	0.636	0.549	0.110	0.551	0.110	5.66	5.57
300	0.424	0.780	0.714	0.584	0.111	0.581	0.110	5.55	5.68

Table 5. Results for Case 1 (*Voltage Profile* 2).

d [m]	*d/DIAG*	μ	*P/dt*	*P/d* (IEEE)	RE_m (IEEE)	*P/d* (FEM)	RE_m (FEM)	Error [%] (IEEE)	Error [%] (FEM)
100	0.141	1.642	0.171	0.310	0.181	0.166	0.115	54.61	1.49
150	0.212	1.588	0.244	0.343	0.149	0.250	0.119	27.54	2.13
200	0.283	1.534	0.305	0.371	0.135	0.310	0.119	15.40	1.70
250	0.354	1.482	0.352	0.396	0.128	0.353	0.118	9.15	0.79
500	0.707	1.258	0.476	0.477	0.118	0.461	0.115	0.77	1.45
1000	1.414	1.003	0.557	0.541	0.116	0.541	0.116	0.94	0.89
1500	2.121	0.883	0.592	0.565	0.115	0.565	0.115	1.33	1.30
3000	4.243	0.743	0.644	0.591	0.115	0.587	0.115	1.65	1.79

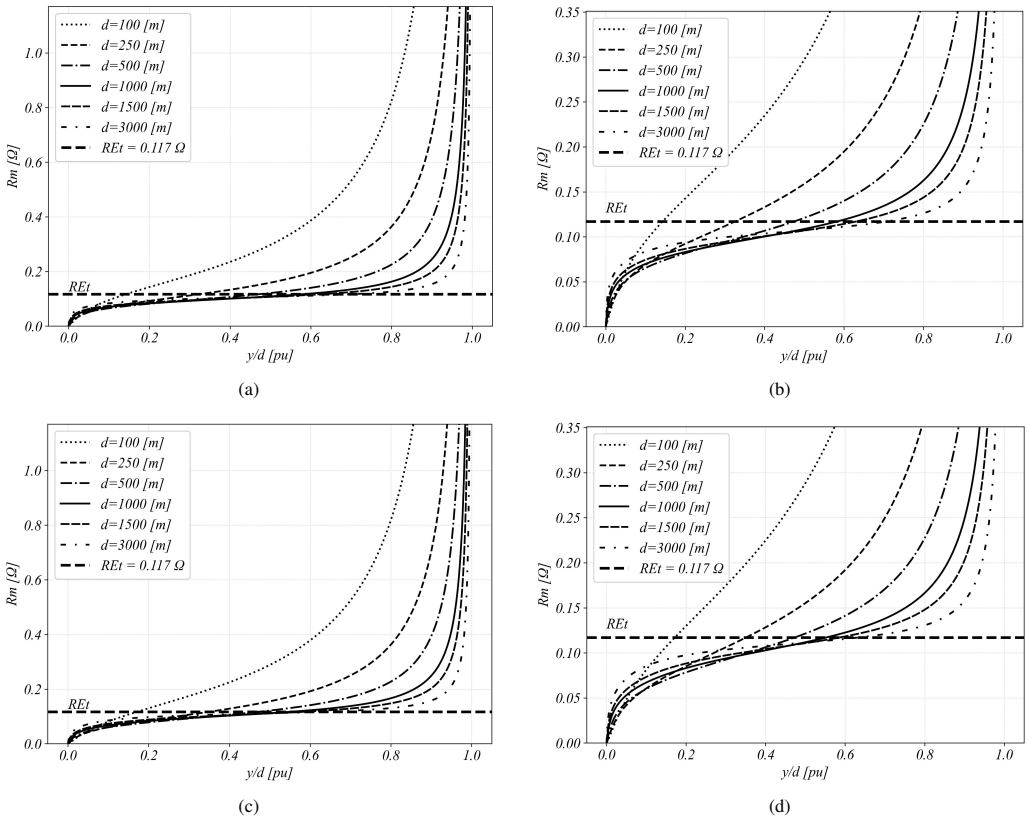

Fig. 12. R_m (*Case 1*) a), c) full fall of the potential profile, b), d) detail near the theoretical resistance intersection.

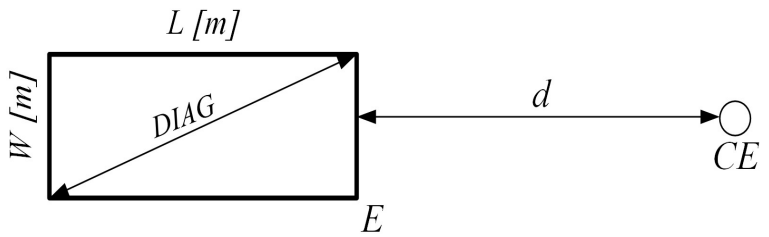

Fig. 13. Visualisation of the *d/DIAG* concept for an equivalent rectangular grounding system.

In conclusion, this case study demonstrates that the proposed methodology is a valid and practical alternative that offers clear advantages over traditional methods under the conditions analysed.

5.3. Case 2: Results

For Case 2, corresponding to a square geometry with L = 1000 m sides ($DIAG$ = 1414 m), the obtained potential profiles are presented in Fig. 14 for the following values of d = {250, 500, 1000, 1500, 3000} m. For this geometry, the resistance value RE_t corresponds to 0.0637 Ω.

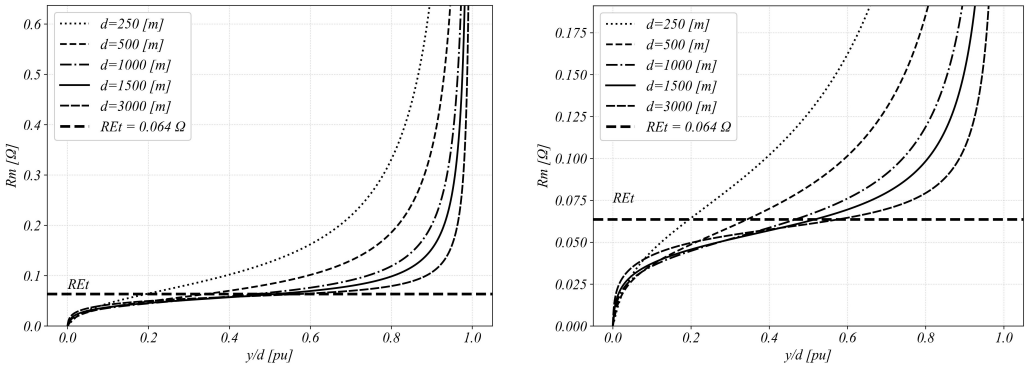

Fig. 14. R_m (*Case* 2): a) full fall of the potential profile, b) detail near the theoretical resistance intersection.

Table 6 summarises the results for Case 2, where the analysis uses the profile that produces the largest errors. As the size of the grounding-system increases (larger *DIAG*), a given *d/DIAG* > 0.14 corresponds to larger absolute distances, placing the measurement point further from the corner and reducing distortion. Consequently, the errors are lower than in Case 1: the maximum remains below 7%, and in most cases stays under 2%.

Table 6. Results for Case 2.

***d* [m]**	***d/DIAG***	***μ***	***P/dt***	***P/d* (IEEE)**	***RE*$_m$ (IEEE)**	***P/d* (FEM)**	***RE*$_m$ (FEM)**	**Error [%] (IEEE)**	**Error [%] (FEM)**
250	0.177	1.610	0.195	0.330	0.088	0.220	0.068	38.19	6.77
500	0.354	1.480	0.344	0.397	0.070	0.355	0.065	9.38	1.89
1000	0.707	1.256	0.468	0.478	0.065	0.462	0.063	1.26	0.76
1500	1.061	1.103	0.518	0.518	0.064	0.513	0.063	0.03	0.44
3000	2.121	0.881	0.579	0.565	0.063	0.566	0.063	0.81	0.79

5.4. Case 3: Results

This case study models a simplified grounding system for a 25–30 MWp PV plant. As shown in Fig. 11, the system comprises five 1000-m branches spaced 500 m apart, connected to a 50 m × 100 m substation grid with a 10 × 20 m mesh (total equivalent *DIAG* ≈ 2300 m). Copper conductors of 10 cm diameter are buried 1 m deep, and the FEM analysis yields a theoretical grounding resistance of RE_t = 0.01770 Ω.

In Figure 15, the measured resistance profiles R_m are shown for different values of d, while Table 7 summarises the main results derived from applying the methodology. It can be observed that, for values of d on the order of 500 m (approximately 0.25 of the system diagonal (*DIAG*)), the corrected methodology already provides an accurate estimate of the grounding resistance of the evaluated system.

Metrol. Meas. Syst., Vol. 33 (2026), No. 1, pp. 1–17
DOI: 10.24425/mms.2026.158373

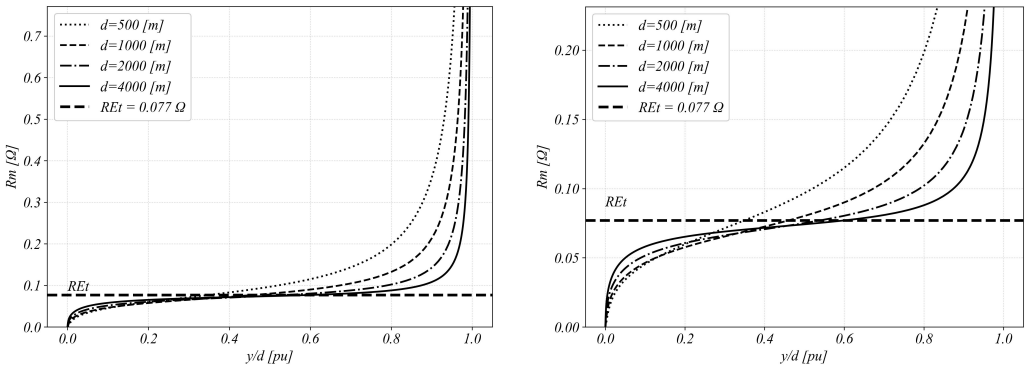

Fig. 15. R_m (Case 3) for various distances d: a) full fall of the potential profile, b) detail the near theoretical resistance intersection.

Table 7. Results for Case 3.

***d* [m]**	***d/DIAG***	***μ***	***P/dt***	***P/d* (IEEE)**	***REm* (IEEE)**	***P/d* (FEM)**	***REm* (FEM)**	**Error [%] (IEEE)**	**Error [%] (FEM)**
500	0.215	1.377	0.349	0.439	0.088	0.413	0.085	14.41	10.16
1000	0.429	1.173	0.461	0.501	0.080	0.491	0.080	4.34	3.25
2000	0.858	0.976	0.541	0.546	0.077	0.548	0.077	0.49	0.58
4000	1.717	0.819	0.603	0.577	0.076	0.575	0.076	0.91	0.99

In summary, three study cases have been evaluated (from FEM simulations) to demonstrate the technical feasibility of the proposed methodology, thus justifying the update of the expression used to determine the position of the potential electrode as a function of μ.

6. Conclusions

Finite element simulations demonstrate that the traditional Tagg Slope Method introduces significant errors when the auxiliary electrode is placed at reduced distances. Two sources dominate these errors: neglecting finite electrode dimensions and using correction curves outside their original validity range. The corrected relationship derived in this work reproduces numerical results with a maximum fitting deviation below 0.02%.

Application to three large grounding systems (500 m square grid, 1000 m square grid, and a photovoltaic-plant grounding system) shows that when measurements avoid corner regions and the auxiliary electrode is located at distances greater than approximately 20% of the system diagonal, the corrected method estimates grounding resistance with typical errors below 3%. For the same conditions, the traditional formulation produces errors ranging from about 10% up to more than 50% when the slope parameter (μ) exceeds 1.4.

For measurements taken near corner regions, errors increase for both methodologies. In these cases, the average errors remain below 5% using the corrected formulation but can exceed 25% with the traditional approach when the auxiliary electrode is placed too close to the grounding system.

The results confirm that the revised formulation extends the reliable use of reduced-distance measurements to very large grounding systems, allowing practical measurements with auxiliary electrode distances on the order of 20% of the system diagonal instead of the several times of the diagonal distance typically required by conventional fall-of-potential methods.

Acknowledgements

I gratefully acknowledge the High Voltage Laboratory at Simón Bolívar University, Caracas, Venezuela, for providing the opportunity to conduct extensive grounding system tests over 20 years. Special thanks to professors Jorge Ramírez, Juan Carlos Rodríguez, and technician Ismael Acosta for their invaluable support.

References

[1] IEEE Guide for Measuring Earth Resistivity, Ground Impedance, and Earth Surface Potentials of a Grounding System. (2012). *IEEE Std 81-2012 (Revision of IEEE Std 81-1983)*, 1–86. https://doi.org/10.1109/ieeestd.2012.6392181

[2] IEEE Guide for Measurement of Impedance and Safety Characteristics of Large, Extended or Interconnected Grounding Systems. (1991). *IEEE Std 81.2-1991*, 1–112. https://doi.org/10.1109/ieeestd.1992.106970

[3] IEEE Approved Draft Guide for Measuring Earth Resistivity, Ground Impedance, and Earth Surface Potentials of a Grounding System. (2025). *IEEE P81/D4, January 2025*, 1–170. https://ieeexplore.ieee.org/document/10945631

[4] Martínez, M. (2014). Methodology based on neural networks for earth resistivity interpretation in congested urban areas. *Ingeniería Energética*, *35*(1), 59–69. http://scielo.sld.cu/pdf/rie/v35n1/rie07114.pdf (in Spanish)

[5] Huang, H., Liu, H., Luo, H., Du, H., Xing, Y., Li, Y., Dawalibi, F. P., Zhou, H., & Fu, L. (2013). Analysis of a large grounding system and subsequent field test validation using the fall of potential method. *Energy and Power Engineering*, *05*(4), 1266–1272. https://doi.org/10.4236/epe.2013.54b240

[6] Leal, A. G., Lazzaretti, A. E., & López-Salamanca, H. L. (2022). A systematic review on grounding impedance measurement in electrical installations. *Electric Power Systems Research*, *214*, 108953. https://doi.org/10.1016/j.epsr.2022.108953

[7] Tagg, G. F. (1964). *Earth Resistances*. The Whitefriars Press Ltd.

[8] Tagg, G. (1969). Measurement of the resistance of an earth-electrode system covering a large area. *Proceedings of the Institution of Electrical Engineers*, *116*(3), 475. https://doi.org/10.1049/piee.1969.0097

[9] Corbellini, G., & Corbellini, U. (1995). Definition and measurement of the earth resistance of an electrode covering a large area. *European Transactions on Electrical Power*, *5*(3), 173–180. https://doi.org/10.1002/etep.4450050305

[10] Raizer, A., Valente, W., & Coelho, V. L. (2017). Development of a new methodology for measurements of earth resistance, touch and step voltages within urban substations. *Electric Power Systems Research*, *153*, 111–118. https://doi.org/10.1016/j.epsr.2017.01.025

[11] Raizer, A., Coelho, V. L., Valente, W., & Cardoso, C. I. (2015). Contribution to TAGG's methodology in the resistance measurement of earth-electrode systems at reduced distances. In *2015 International Symposium on Lightning Protection (XIII SIPDA)* (pp. 109–115). https://doi.org/10.1109/sipda.2015.7339307

[12] Alcantara, F. R. (2018). An approximated procedure to find the correct measurement point in the Fall-of-Potential method. In *IEEE PES Transmission & Distribution Conference and Exhibition - Latin America (T&D-LA)* (pp. 1–5). https://doi.org/10.1109/tdc-la.2018.8511738

[13] Moreno, J., Simón, P., Faleiro, E., García, D., Denche, G., & Asensio, G. (2024). A simple procedure to obtain the grounding resistance measurement of very large and urban electrodes by a modified Fall-of-Potential method. *Applied Sciences*, *14*(17), 8040. https://doi.org/10.3390/app14178040

[14] Berberović, S., & Boras, V. (2000). Correction of resistance measurement of large grounding systems. *European Transactions on Electrical Power*, *10*(2), 105–111. https://doi.org/10.1002/etep.4450100207

[15] Sunjerga, A., Rachidi, F., Rubinstein, M., & Poljak, D. (2018). Calculation of the grounding resistance of structures located on elevated terrain. *IEEE Transactions on Electromagnetic Compatibility*, *61*(6), 1891–1895. https://doi.org/10.1109/temc.2018.2877214

[16] Sunjerga, A., Rubinstein, M., Poljak, D., Karami, H., & Rachidi, F. (2020). Grounding resistance of a hemispheric electrode located on the top of a finite-height, cone-shaped mountain. *IEEE Transactions on Electromagnetic Compatibility*, *62*(5), 1889–1892. https://doi.org/10.1109/temc.2020.2974579

[17] Omar, R., Rani, M. A., Yunus, M. A., Isa, A. a. M., Mirza, W. I. I. W. I., Zin, M. S. M., & Roslan, L. (2018). Investigation of Mesh Size Effect on Dynamic Behaviour of an Assembled Structure with Bolted Joints using Finite Element Method. *International Journal of Automotive and Mechanical Engineering*, *15*(3), 5695–5708. https://doi.org/10.15282/ijame.15.3.2018.22.0437

[18] Silvester, P. P., & Ferrari, R. L. (1996). Finite Elements for Electrical Engineers. In *Cambridge University Press eBooks*. https://doi.org/10.1017/cbo9781139170611

[19] Sorgente, T., Vicini, F., Berrone, S., Biasotti, S., Manzini, G., & Spagnuolo, M. (2024). Mesh optimization for the virtual element method: How small can an agglomerated mesh become? *Journal of Computational Physics*, *521*, 1–20. https://doi.org/10.1016/j.jcp.2024.113552

[20] Megger. (2021). *Getting Down to Earth: A Practical Guide to Earth Resistance Testing*. https://www.megger.com/sites/g/files/utfabz201/files/acquiadam_assets/2021-04/GDTE_en.pdf

Miguel Martínez Lozano holds B.Sc. and M.Sc. degrees in electrical engineering from Simón Bolívar University (Venezuela) and a Ph.D. from the Technical University of Madrid (Spain). He has held academic and research positions at Simón Bolívar University and De La Salle Bajío University. He is currently a Lecturer at the Technical University of Madrid. His research focuses on electromagnetic transients, insulation coordination, high voltage engineering, and dielectric behaviour.